

# A comparative analysis for different finite element types in strain-gradient elasticity simulations performed on Firedrake and FEniCS

B. Cagri Sarar<sup>a</sup>, M. Erden Yildizdag<sup>b,c</sup>, Francesco Fabbrocino<sup>d</sup>, B. Emek Abali<sup>e,\*</sup>

<sup>a</sup>*International Research Center on Mathematics and Mechanics of Complex Systems, University of L'Aquila, L'Aquila, Italy*

<sup>b</sup>*Department of Architecture, Design and Urban Planning, University of Sassari, 07041 Alghero, Italy*

<sup>c</sup>*Faculty of Naval Architecture and Ocean Engineering, Istanbul Technical University, 34469 Istanbul, Turkey*

<sup>d</sup>*Department of Engineering, Telematic University Pegaso, 80143 Napoli, Italy*

<sup>e</sup>*Department of Materials Science and Engineering, Division of Applied Mechanics, Uppsala University, Box 35, 751 03 Uppsala, Sweden*

---

## Abstract

The layer-upon-layer approach in additive manufacturing, open or closed cells in polymeric or metallic foams involve an intrinsic microstructure tailored to the underlying applications. Homogenization of such architected materials creates metamaterials modeled by higher-gradient models, specifically when the microstructure's characteristic length is comparable to the length scale of the structure. In this study, we conduct a comparative analysis of various finite elements methods for solving problems in strain-gradient elasticity. We employ open-source packages from Firedrake and FEniCS. Different finite element formulations are tested: we implement Lagrange, Argyris, Hermite elements, a Hu–Washizu type (mixed) formulation, as well as isogeometric analysis with Non-Uniform Rational B-Splines (NURBS). For the numerical study, we investigate one- and two-dimensional problems discussed in the literature of strain-gradient modeling. All developed codes are open-access to encourage research in Finite Element Method (FEM) based computation of generalized continua.

*Keywords:* Strain-gradient elasticity; Finite element method; Variational methods; Higher-gradient modeling

*2010 MSC:* 00-01, 99-00

---

## 1 Introduction

Owing to its innovative process, additive manufacturing (AM) facilitates the fabrication of extraordinary structures, thereby providing engineers an opportunity to envision and explore diverse perspectives in design and manufacturing [1, 2, 3]. In particular, the layer-by-layer production technique offered by AM enables the creation of intricate internal patterns, controlling and enhancing the functionality of the manufactured components (for example, see recent studies [4, 5, 6]). Therefore, the ability to adjust infill patterns [7, 8, 9] and modify infill ratios [10, 11, 12] has become pivotal in shaping the internal structural design of multi-scale structures [13, 14, 15]. This functionality not only enables engineers to fine-tune the mechanical properties and performance

---

\*Corresponding author

*Email address:* bilenemek@abali.org (B. Emek Abali)

characteristics of manufactured components; but also empowers them to optimize material usage and reduce manufacturing costs.

Designing and fabricating complex materials using AM clearly necessitates novel mathematical models for assessing the overall behavior under various conditions. As classical mathematical models fall short in accurately predicting the behavior of multi-scale structures, alternative advanced modeling techniques, which require proper generalization of classical elasticity theory, are currently drawing great deal of interest (see recent applications in [16, 17, 18]). Particularly, micropolar [19, 20, 21], micromorphic [22, 23, 24], Cosserat [25, 26, 27], strain-gradient [28, 29, 30, 31] continua are extensively investigated to model complex problems providing efficient numerical simulations. Notably, to establish such models, variational methods [32, 33, 34] are quite powerful, providing a systematic approach to study higher gradient theories [35, 36, 37, 38]. Basically, these variational frameworks involve defining an appropriate action functional, which encapsulates the physical properties and constraints of the system under consideration. By processing the action functional concerning the relevant fields, such as displacement, strain, or other relevant entities, one may derive the Euler–Lagrange equations that govern the problem under investigation [39, 40]. Specifically, in the context of strain-gradient modeling, the action functional depends on not only the strain but also its gradient. This extension may be motivated by an upscaling from a discrete system with non-local connection [41] or continuum setting starting from Cauchy continuum [42].

In addition to modeling, effective numerical simulation of such complex models is also of great interest to provide reliable predictions. In this study, we present an in-depth comparative analysis for the numerical simulation of strain-gradient models, considering different finite element formulations. To this end, two benchmark problems are investigated that are available in the literature, by utilizing packages from FEniCS and Firedrake, open-source finite element computing platforms. In each case, the problem is simulated using various shape functions, including Lagrange, Argyris, Hermite elements, a mixed FE formulation, and NURBS-based isogeometric analysis (IGA). We investigate FE solution of a two-dimensional simple shear problem discussed in [43] and a one-dimensional pull-out problem numerically studied in [44]. For the FE analysis, a discrete approximation of continuous functions are used in order to solve a variational formulation that is challenging to adequately represent by a suitable function space. Hence, there are different suggestions in the literature. Firedrake and FEniCS are using modern techniques with high level scripting to solve any formulation that automates the numerical solution of field equations with the chosen element type and formulation. Specifically herein,  $C^1$  continuous elements [45], and isogeometric analysis (IGA) as function spaces are rather simple to utilize by leveraging the domain-specific language of the FEniCS project [46]. FE method is based on a compact support with elements only locally effective such that a monotonous convergence is guaranteed. Yet higher order formulations are often defined within the whole domain (sometimes called patch) such that reliability and error estimation may be in danger. One example of nonlocal formulation is the so-called isogeometric analysis (IGA), where field equations are mapped to a parametric reference domain, and solutions are approximated using function spaces constructed from linear combinations of finite element basis functions over that domain [47]. IGA has been extensively applied into different fields (for example, see [48, 49, 50]). In this work, we use the library called tIGAr [51] available within the open-source finite element automation software FEniCS. It employs a global version of Bézier extraction to integrate FEniCS’s capabilities into IGA workflows. Furthermore, with the aid of Firedrake platform, we exploit Argyris and Hermite, which are higher-order elements. Another possibility is to increase the number of field equations such that the smoothness conditions are reduced leading to a mixed formulation.

The rest of the study is as follows. In Section 2, the adapted problems and their strain-gradient

models are summarized. In Section 3, the conducted comparative analysis is demonstrated and discussed in detail, assessing the different FE formulations. Finally, conclusions are drawn in Section 4.

## 2 Method of solution in strain-gradient elasticity

The strain-gradient model [52] is adapted in the numerical simulations and summarized in this part. Following the variational framework presented in [53], we consider the Lagrange function depending on displacement and its first and second gradients in space and time, as follows:

$$\mathcal{L} = \frac{1}{2}\rho_0(\dot{u}_i\dot{u}_i + d^2\dot{u}_{i,j}\dot{u}_{i,j} + \tau^2\ddot{u}_i\ddot{u}_i) - w + \rho_0(f_i u_i + \ell_{ij} u_{i,j}) \quad (1)$$

where we understand Einstein summation convention over the repeated indices,  $i, j, k, \dots \in [1, 2, 3]$  in three-dimensional space,  $\rho_0$  is the mass density of the material, and  $\mathbf{u}$  is the displacement, defined by difference between the current position,  $\mathbf{x}$ , and the reference position,  $\mathbf{X}$ . The first term in the Lagrangian density is the kinetic energy density, including a length scale,  $d$  (in meter), and a relaxation time,  $\tau$  (in second). The second term,  $w$ , is the deformation energy density, which is a function of the linearized Green–Lagrange strain and its gradient,  $w = \hat{w}(\boldsymbol{\varepsilon}, \nabla\boldsymbol{\varepsilon})$ . The last term in the Lagrangean density represents the energy density due to the volumetric effects, including a body force density,  $\mathbf{f}$ , and a supply term,  $\boldsymbol{\ell}$ , which is accounted for work through displacement gradient. The linearized strain tensor and its gradient are defined by

$$\varepsilon_{ij} = \frac{1}{2}(u_{i,j} + u_{j,i}), \quad \varepsilon_{ij,k} = \frac{1}{2}(u_{i,jk} + u_{j,ik}) \quad (2)$$

where

$$u_{i,j} = \frac{\partial u_i}{\partial X_j}, \quad u_{i,jk} = \frac{\partial^2 u_i}{\partial X_k \partial X_j}. \quad (3)$$

The deformation energy density is given by

$$w = \frac{1}{2}\varepsilon_{ij} C_{ijkl} \varepsilon_{kl} + \frac{1}{2}\varepsilon_{ij,k} D_{ijklmn} \varepsilon_{lm,n} + \varepsilon_{ij} G_{ijklm} \varepsilon_{kl,m}, \quad (4)$$

where the rank-4 tensor,  $C_{ijkl}$ , corresponds to first-gradient (strain related) elastic properties. For isotropic materials, it reads

$$C_{ijkl} = c_1 \delta_{ij} \delta_{kl} + c_2 (\delta_{ik} \delta_{jl} + \delta_{il} \delta_{jk}). \quad (5)$$

The rank-6 tensor,  $D_{ijklmn}$ , represents second-gradient (strain gradient related) elastic properties, again for isotropic materials,

$$D_{ijklmn} = c_3 (\delta_{ij} \delta_{kl} \delta_{mn} + \delta_{in} \delta_{jk} \delta_{lm} + \delta_{ij} \delta_{km} \delta_{ln} + \delta_{ik} \delta_{jn} \delta_{lm}) + c_4 \delta_{ij} \delta_{kn} \delta_{ml} \quad (6)$$

$$+ c_5 (\delta_{ik} \delta_{jl} \delta_{mn} + \delta_{im} \delta_{jk} \delta_{ln} + \delta_{ik} \delta_{jm} \delta_{ln} + \delta_{il} \delta_{jk} \delta_{mn}) + c_6 (\delta_{il} \delta_{jm} \delta_{kn} + \delta_{im} \delta_{jl} \delta_{kn}) \quad (7)$$

$$+ c_7 (\delta_{il} \delta_{jn} \delta_{mk} + \delta_{im} \delta_{jn} \delta_{lk} + \delta_{in} \delta_{jl} \delta_{km} + \delta_{in} \delta_{jm} \delta_{kl}). \quad (8)$$

Strain gradient is coupled to strain via the rank-5 tensor,  $G_{ijklm}$ , which vanishes for a centrosymmetric microstructure. Also,  $c_1$  and  $c_2$  are first-gradient constitutive parameters while  $c_3, c_4, c_5, c_6,$  and  $c_7$  are strain-gradient constitutive parameters.

Next, the following action functional is postulated in space (3-D) and time spanning an infinitesimal element,  $d\Sigma = dV dt$ , for volume and time; as well as an infinitesimal element,  $d\Gamma = dA dt$ , for surface and time; and herein,  $d\Pi = d\ell dt$ , for line (edge) and time, as follows:

$$\mathcal{A} = \int_{\Omega} \mathcal{L} d\Sigma + \int_{\partial\Omega} W_s d\Gamma + \int_{\partial\partial\Omega} W_e d\Pi \quad (9)$$

where  $W_s$  and  $W_e$  are energy densities defined, respectively, over the surface  $\partial\Omega$  and the edge  $\partial\partial\Omega$  of the domain of interest  $\Omega$ . These so-called NEUMANN boundaries are given. We neglect the inertial terms in this study and compute cases in statics such that the time integration drops. Then, the variation of the energy reads

$$\begin{aligned} \delta\mathcal{A} = & \int_{\Omega} \left( \rho_0 f_i \delta u_i + \rho_0 \ell_{ij} \delta u_{i,j} - \frac{\partial w}{\partial u_{i,j}} \delta u_{i,j} - \frac{\partial w}{\partial u_{i,jk}} \delta u_{i,jk} \right) dV \\ & + \int_{\partial\Omega} \left( \frac{\partial W_s}{\partial u_i} \delta u_i + \frac{\partial W_s}{\partial u_{i,j}} \delta u_{i,j} \right) dA + \int_{\partial\partial\Omega} \frac{\partial W_e}{\partial u_i} \delta u_i d\ell . \end{aligned} \quad (10)$$

A vanishing action leads to the solution according to NOETHER's theorem [54]. The test function,  $\delta\mathbf{u}$ , is arbitrary and chosen to vanish on the DIRICHLET boundaries, where the primitive variables are known. Both  $\mathbf{u}$  and  $\delta\mathbf{u}$  are from same space known as the GALERKIN approach. The derivative of the stored energy density with respect to the first gradient of displacement and the second gradient of displacement are derived as follows

$$\frac{\partial w}{\partial u_{i,j}} = \frac{\partial w}{\partial \varepsilon_{kl}} \frac{\partial \varepsilon_{kl}}{\partial u_{i,j}} = \frac{\partial w}{\partial \varepsilon_{kl}} \frac{1}{2} (\delta_{ki} \delta_{lj} + \delta_{kj} \delta_{li}) = C_{ijkl} \varepsilon_{kl}, \quad (11)$$

$$\frac{\partial w}{\partial u_{i,jk}} = \frac{\partial w}{\partial \varepsilon_{lm,n}} \frac{\partial \varepsilon_{lm,n}}{\partial u_{i,jk}} = \frac{\partial w}{\partial \varepsilon_{lm,n}} \frac{1}{2} (\delta_{li} \delta_{mj} \delta_{nk} + \delta_{mi} \delta_{lj} \delta_{nk}) = D_{ijklmn} \varepsilon_{lm,n}, \quad (12)$$

by considering the symmetry of the stiffness tensors ( $C_{ijkl} = C_{jikl} = C_{klij} = C_{klji}$ ) and ( $D_{lmnijk} = D_{lmnjik} = D_{ijklmn} = D_{jiklmn}$ ).

In order to perform simulations with different finite element formulations, Eq. (10) is utilized in FEniCS and Firedrake. Neglecting inertial terms, body forces, and work on edge and surface due to second gradient terms, Eq. (10) takes the following form:

$$\int_{\Omega} (\delta u_{i,j} C_{ijkl} \varepsilon_{kl} + \delta u_{i,jk} D_{ijklmn} \varepsilon_{lm,n}) dV = \int_{\partial\Omega} \hat{t}_i \delta u_i dA, \quad (13)$$

where  $\hat{\mathbf{t}}$  is the traction given on boundaries.

One possible approach is to use sufficiently smooth elements for  $\mathbf{u}$ . In this case, for applying boundary conditions (i.e. prescribed displacement, prescribed displacement gradient, and applied tractions on both boundary and edge), the penalty method is utilized in the simulations. To properly enforce the boundary conditions while using IGA, Argyris and Hermite elements, Eq. (13) results in

$$\int_{\Omega} (\delta u_{i,j} C_{ijkl} \varepsilon_{kl} + \delta u_{i,jk} D_{ijklmn} \varepsilon_{lm,n}) dV = \int_{\partial\Omega_N} \hat{t}_i \delta u_i dA + \int_{\partial\Omega_D} K (u_i - \hat{u}_i) \delta u_i dA, \quad (14)$$

with given Neumann boundaries,  $\hat{\mathbf{t}}$ , and Dirichlet boundaries,  $\hat{\mathbf{u}}$ . The implementation of Dirichlet boundaries is employed in the integral form by means of a large number,  $K$ , also called penalty factor. This fact is needed owing to higher continuity of the element at the domain boundaries.

Another possibility is to introduce the mixed FE formulation [43] with an additional unknown,  $g_{ij}$ , imposing  $u_{i,j} = g_{ij}$ , through Lagrange multipliers as follows:

$$\int_{\Omega} \left( \delta u_{i,j} C_{ijkl} \varepsilon_{kl} + \delta g_{ij,k} D_{ijklmn} \varepsilon_{lm,n} + L_{ij} (\delta g_{ij} - \delta u_{i,j}) + (g_{ij} - u_{i,j}) \delta L_{ij} \right) dV = \int_{\partial\Omega_N} \hat{t}_i \delta u_i dA, \quad (15)$$

where

$$\varepsilon_{ij} = \frac{1}{2}(u_{i,j} + u_{j,i}), \quad \varepsilon_{ij,k} = \frac{1}{2}(g_{ij,k} + g_{ji,k}). \quad (16)$$

In this version, Dirichlet boundaries are implemented directly by taking them out of the matrices after assembly in the finite element method.

## 2.1 2-D simple shear problem

The first strain-gradient model examined in this study is the 2-D simple shear of a plate of length  $L$  and height  $H$ , which was investigated both numerically and analytically by Shekarchizadeh et al. [43]. The general analytical solution in closed form is provided below,

$$u = u_x(y) = q_1 + q_2 y + q_3 \sinh\left(\frac{y}{r}\right) + q_4 \cosh\left(\frac{y}{r}\right) \quad (17)$$

where  $r = \sqrt{\frac{(c_5+c_6+c_7)}{c_2}}$  with integration constants  $q_1, q_2, q_3, q_4$ . We study 2 cases:

- case D: the prescribed displacement:

$$q_1 = 0, \quad q_2 = \frac{\hat{u} \cosh\left(\frac{H}{r}\right)}{H \cosh\left(\frac{H}{r}\right) - r \sinh\left(\frac{H}{r}\right)}, \quad q_3 = \frac{\hat{u} r}{r \sinh\left(\frac{H}{r}\right) - H \cosh\left(\frac{H}{r}\right)}, \quad q_4 = 0 \quad (18)$$

- case T: the applied traction:

$$q_1 = \frac{-r^3 \hat{t} \sinh\left(\frac{H}{r}\right)}{s}, \quad q_2 = \frac{r^2 \hat{t} \cosh\left(\frac{H}{r}\right)}{s}, \quad q_3 = \frac{-r^3 \hat{t} \cosh\left(\frac{H}{r}\right)}{s}, \quad q_4 = \frac{r^3 \hat{t} \sinh\left(\frac{H}{r}\right)}{s} \quad (19)$$

where

$$s = c_2 r^2 \left( \cosh\left(\frac{H}{r}\right) - 1 \right) + c_5 + c_6 + c_7. \quad (20)$$

As schematically shown in Fig. 1, for case D in Fig. 1a) and case T in Fig. 1b), the difference between these cases is obvious at the bottom edge. In case D, the bottom edge may rotate, while in case T, it is clamped.

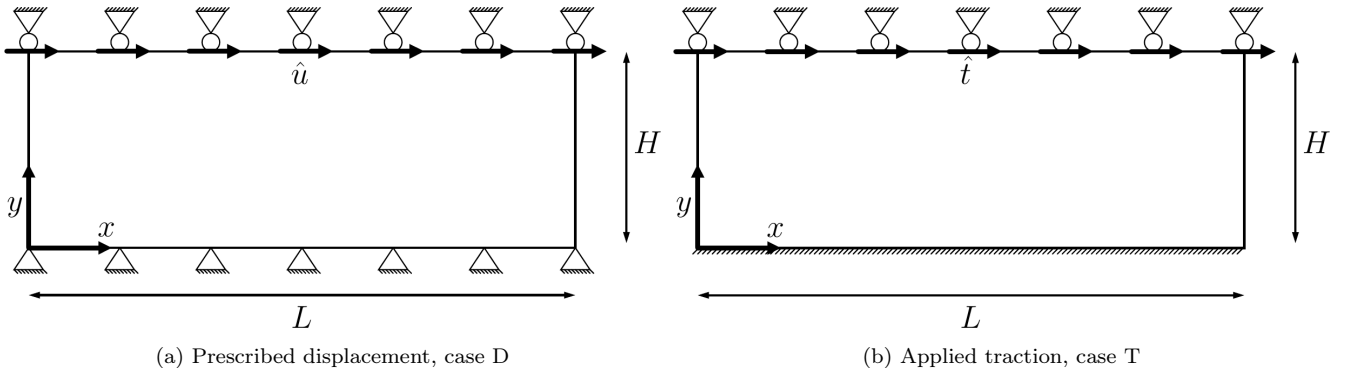


Figure 1: 2-D simple shear problem for solving by the strain-gradient formulation with two separate boundary conditions.

For the prescribed displacement, case D, a displacement of  $\hat{\mathbf{u}}$  is applied at the top edge by a rail such that the displacement gradient is set to zero in order to illuminate the effects of strain-gradient terms. While the bottom edge prevents a translation but not rotation. For this case, the weak form reads

$$\begin{aligned} \int_{\Omega} \left( \delta u_{i,j} C_{ijkl} \varepsilon_{kl} + \delta u_{i,j,k} D_{ijklmn} \varepsilon_{lm,n} \right) dV &= \int_{\partial\Omega_{\text{bot}}} K(u_i - \hat{u}_i^{\text{bot}}) \delta u_i dA \\ &+ \int_{\partial\Omega_{\text{top}}} \left( K(u_i - \hat{u}_i^{\text{top}}) \delta u_i + K(u_{i,j} - \hat{g}_{ij}^{\text{top}}) \delta u_{i,j} \right) dA \end{aligned} \quad (21)$$

where all terms with hat,  $\hat{\mathbf{u}}^{\text{bot}} = 0$ ,  $\hat{\mathbf{u}}^{\text{top}}$ ,  $\hat{\mathbf{g}}^{\text{top}} = 0$ , are given to prescribe displacement.

For the applied traction, case T, a traction,  $\hat{\mathbf{t}}$  is applied at the top edge, while the displacement and displacement gradient are fixed to zero at the bottom edge,

$$\begin{aligned} \int_{\Omega} \left( \delta u_{i,j} C_{ijkl} \varepsilon_{kl} + \delta u_{i,j,k} D_{ijklmn} \varepsilon_{lm,n} \right) dV &= \int_{\partial\Omega_{\text{top}}} \hat{t}_i \delta u_i dA \\ &+ \int_{\partial\Omega_{\text{top}}} K(u_1 - \hat{u}_1^{\text{top}}) \delta u_1 dA + \int_{\partial\Omega_{\text{bot}}} \left( K(u_i - \hat{u}_i^{\text{bot}}) \delta u_i + K(u_{i,j} - \hat{g}_{ij}^{\text{bot}}) \delta u_{i,j} \right) dA \end{aligned} \quad (22)$$

although written explicitly,  $\hat{u}_1^{\text{top}} = 0$ ,  $\hat{\mathbf{u}}^{\text{bot}} = 0$ ,  $\hat{\mathbf{g}}^{\text{bot}} = 0$ , setting all components zero ensure no deformation and no rotation along the bottom edge.

Importantly, periodic boundary conditions are imposed to the lateral boundaries of the plate, effectively rendering the plate's length negligible.

## 2.2 1-D pull-out problem

The pull-out problem is the second strain-gradient model examined in this study by following Rezaei et al. [44]. As shown in Fig. 2, the pull-out test is an extraction of a rebar (reinforced rod) from a cylindrical block of radius  $R$ . By following Rezaei et al. [44], the axisymmetric 3-D problem is simplified to formulate a 1-D model. Here, the assumptions are: (i) external surface of the cylindrical block is fixed; (ii) cylindrical block is infinitely long to neglect boundary effects and have displacement field uniform in circumferential direction; (iii) the imposed displacement applied to rigid bar ( $\hat{u}_p$ ) is axially directed and the radius of the rigid bar,  $\varepsilon$ , goes to zero.

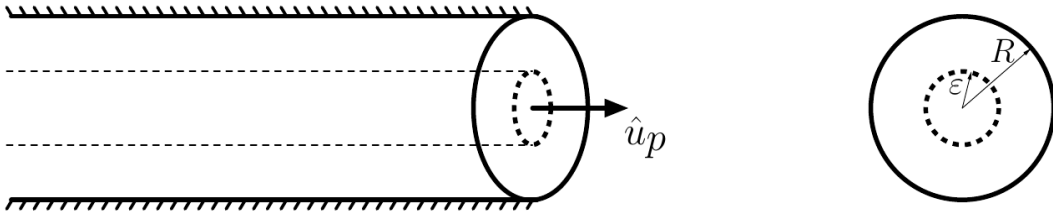


Figure 2: The pull-out problem, a prescribed displacement,  $\hat{u}_p$ , pulls the rebar from the cylindrical bulk of radius  $R$  clamped around the surface (skin) area.

For a solution, the system is reduced to a 1-D formulation by utilizing cylindrical polar coordinates,  $(r, \theta, z)$ , such that the quadratic deformation energy reads in Green–Lagrange strain and

their gradients,

$$\begin{aligned}
w(u_z, u'_z, u''_z) &= \frac{c_1}{8} (u'_z)^4 + c_2 \left( \frac{(u'_z)^2}{2} + \frac{(u'_z)^4}{4} \right) \\
&+ \frac{c_3}{2r} \left( (u'_z)^2 u''_z + (u'_z + 2ru''_z) \right) + 2c_4 (u'_z)^2 (u''_z)^2 \\
&+ \frac{c_5}{4r^2} \left( (u'_z)^2 (1 + 4r^2 (u''_z)^2) + r^2 (u''_z)^2 + 4r (u'_z)^3 u''_z + 2ru'_z u''_z + (u'_z)^4 \right) \\
&+ \frac{c_6}{2r^2} \left( (u'_z)^2 (2r^2 (u''_z)^2 + 1) + r^2 (u''_z)^2 + (u'_z)^4 \right) \\
&+ \frac{c_7}{4r^2} \left( (u'_z)^2 (4r^2 (u''_z)^2 + 1) + r^2 (u''_z)^2 + (u'_z)^4 \right)
\end{aligned} \tag{23}$$

where  $c_1$  and  $c_2$  are the first-gradient parameters (i.e., Lamé parameters), and  $c_3, c_4, c_5, c_6,$  and  $c_7$  are second-gradient parameters. Also,  $u_z$  represents the axial displacement. Considering the analogous variational formulation, we obtain

$$\delta \mathcal{A} = 0 \int_{\Omega} \left( \frac{\partial w}{\partial u_z} \delta u_z + \frac{\partial w}{\partial u'_z} \delta u'_z + \frac{\partial w}{\partial u''_z} \delta u''_z \right) dV . \tag{24}$$

By calculating each term,

$$\begin{aligned}
\frac{\partial w}{\partial u_z} &= 0, \\
\frac{\partial w}{\partial u'_z} &= \frac{\lambda}{2} ((u'_z)^3) + \mu ((u'_z) + (u'_z)^3) + \frac{c_3}{2z} (3(u'_z)^2 u'' + 4z(u'_z)(u''^2)) + 2c_4 (2(u'_z)(u''^2)) \\
&+ \frac{c_5}{4z^2} \left( 2(u'_z) + 8z^2(u'_z)u''(u'_z)^2 + 12z(u'_z)^2 u''(u'_z) + 2zu'' + 4(u'_z)^3 \right) \\
&+ \frac{c_6}{2z^2} (4z^2(u'_z)(u''^2) + 2(u'_z) + 4(u'_z)^3) + \frac{c_7}{4z^2} (8z^2(u'_z)(u''^2) + 2(u'_z) + 4(u'_z)^3), \\
\frac{\partial w}{\partial u''_z} &= \frac{c_3}{2z} ((u'_z)^3 + 4zu''(u'_z)^2) + 2c_4 (2u''(u'_z)^2) \\
&+ \frac{c_5}{4z^2} \left( 8z^2(u'_z)^2 u'' + 2z^2 u'' \delta u''_z + 4z(u'_z)^3 + 2z(u'_z) + 4(u'_z)^3 \right) \\
&+ \frac{c_6}{2z^2} (4z^2(u'_z)^2 u'' + +2z^2 u'') + \frac{c_7}{4z^2} (8z^2(u'_z)^2 u'' + +2z^2 u'').
\end{aligned} \tag{25}$$

We stress that the adapted 1-D strain-gradient model is non-linear without an analytical solution as opposed to the 2-D strain-gradient model presented for the simple shear problem with the aforementioned analytical solution.

### 3 Numerical results and discussion

For the numerical simulations of the 2-D strain-gradient model, we consider a plate of length  $L = 1.5$  mm and height  $H = 0.5$  mm. The constitutive parameters adapted in the simulations are listed in Table 1, considering a material of Young's modulus  $E = 400$  MPa and Poisson's ratio  $\nu = 0.49$ . All the constitutive parameters, including those for the strain-gradient elasticity contribution,

are based on the granular micromechanics modeling by Barchiesi et al. [55], given by,

$$\begin{aligned}
c_1 &= \frac{E\nu}{(1+\nu)(1-2\nu)} \\
c_2 &= \frac{E}{2(1+\nu)} \\
c_3 = c_4 &= \frac{l_c^2}{112}\lambda \\
c_5 = c_7 &= \frac{l_c^2}{1120}(7\mu + 3\lambda) \\
c_6 &= \frac{l_c^2}{1120}(7\mu - 4\lambda) ,
\end{aligned} \tag{26}$$

where the characteristic length,  $l = 0.1$  for case D and  $l = 0.2$  for case T, represents the size of microstructural interactions.

The parameters  $c_1$  and  $c_2$  compensate the negative values  $c_3, c_4, c_5, c_6, c_7$ , we emphasize that the presence of negative values is a known fact [56] and still resembles a positive energy, thereby guaranteeing a unique solution. This aspect is elaborately discussed in the context of positive definiteness in strain-gradient theory [57, 58, 59].

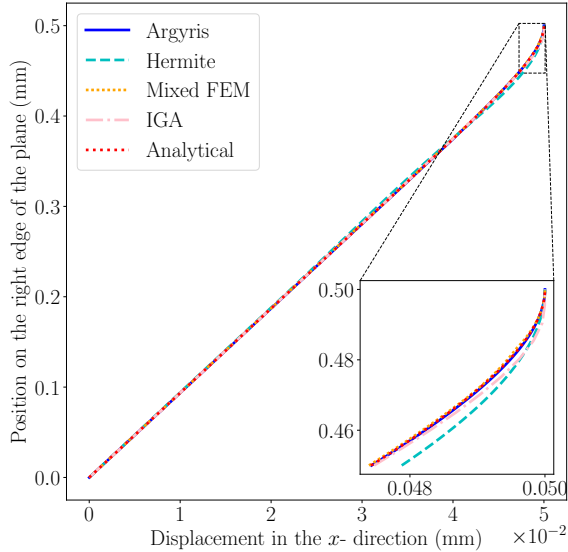
Table 1: Constitutive parameters adapted for the simple shear problem.

| $c_1$ in MPa | $c_2$ in MPa | $c_3$ in N | $c_4$ in N | $c_5$ in N | $c_6$ in N | $c_7$ in N |
|--------------|--------------|------------|------------|------------|------------|------------|
| 6577.18      | 134.23       | 0.59       | 0.59       | 0.18       | -0.23      | 0.18       |

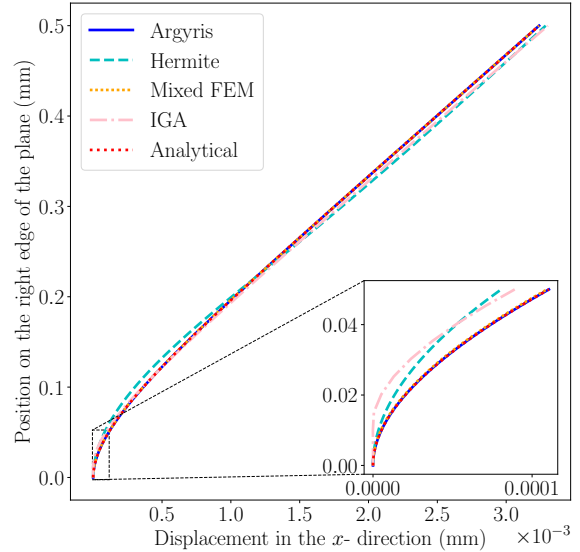
The simple shear problem is investigated for the cases D and T, prescribed displacement and applied traction, respectively. In the case D,  $\hat{\mathbf{u}} = (0.05, 0)$  in mm is applied for a horizontal displacement of the top edge of the plate. In the second case, a traction vector,  $\hat{\mathbf{t}} = (1, 0)$  in N/mm, applied for a horizontal shear to the same (top) edge. In Fig. 3, the numerical predictions obtained by the performed finite element simulations are compared to the analytical solution for both cases. The provided plots are the displacement in the horizontal direction occurring along the right edge of the plate. The zoomed-in sections highlight the predicted displacements and the accuracy of the approximations. Notably, the applied zero displacement gradient conditions in both cases, the top edge for the prescribed displacement case and the bottom edge for the applied traction case, are accurately captured in the finite element simulations.

In general, numerical predictions are consonant with the analytical solution in both cases. Precisely, for the case D, obviously, Argyris and the mixed FE simulations provide a convincing match against the analytical solution, while Hermite and IGA simulations provide slightly different predictions, around the top edge of the plate. On the other hand, for the applied traction case, a similar trend is observed, having negligible differences around the bottom edge of the plate. The discretization of the presented results in Fig. 3 have been selected based on convergence behavior of each formulation. For the simulations with the Argyris and Hermite elements, the rectangular domain is discretized into 54 triangular elements that is 612 Degrees Of Freedom (DOF) and 96 triangular elements that is 552 DOF triangular elements, respectively. A single 2nd-degree NURBS patch with 100 elements (882 DOF) is used for the IGA simulation. And, to perform the mixed FEM simulation, the domain is discretized into 5400 linear elements (54720 DOF).





(a) Prescribed displacement case.



(b) Applied traction case.

Figure 3: Comparison of the converged results for the simple shear problem.

Furthermore, to investigate the convergence characteristics of different FE formulations, a series of simulations is designed, refining the computational domain systematically as known as  $h$ -convergence. The computed errors are presented as a function of degrees of freedom on a log-log scale using  $L_1$  error norm for both cases in Fig. 4, calculated by

$$\text{Error} = \int_0^1 |u^{\text{ref}} - u^{\text{sim}}| dx \approx \sum_{i=0}^{N-2} \frac{1}{2} (|u_i^{\text{ref}} - u_i^{\text{sim}}| + |u_{i+1}^{\text{ref}} - u_{i+1}^{\text{sim}}|) \Delta x \quad (27)$$

using the trapezoidal integration method and considering the analytic solution,  $u^{\text{ref}}$  and the numerical solution,  $u^{\text{sim}}$ , in 1-D reduced order model. The error calculation involves defining the distance  $\Delta x$  as  $\frac{1}{N-1}$ , where  $N$  represents the number of calculated displacement values.

In the simulations with Argyris and the mixed FE, we observe a monotonous convergence. As expected, Argyris elements have a higher convergence rate compared to the mixed FE with an adequate accuracy and efficiency compared with the analytical solution. Remarkably, not ideal convergence characteristics are obtained for Hermite elements and IGA, with increasing number of degrees of freedom. Especially, the simulations with Hermite elements show an undesirable convergence behavior in both cases such that a posteriori error estimation is not possible without knowing the solution.

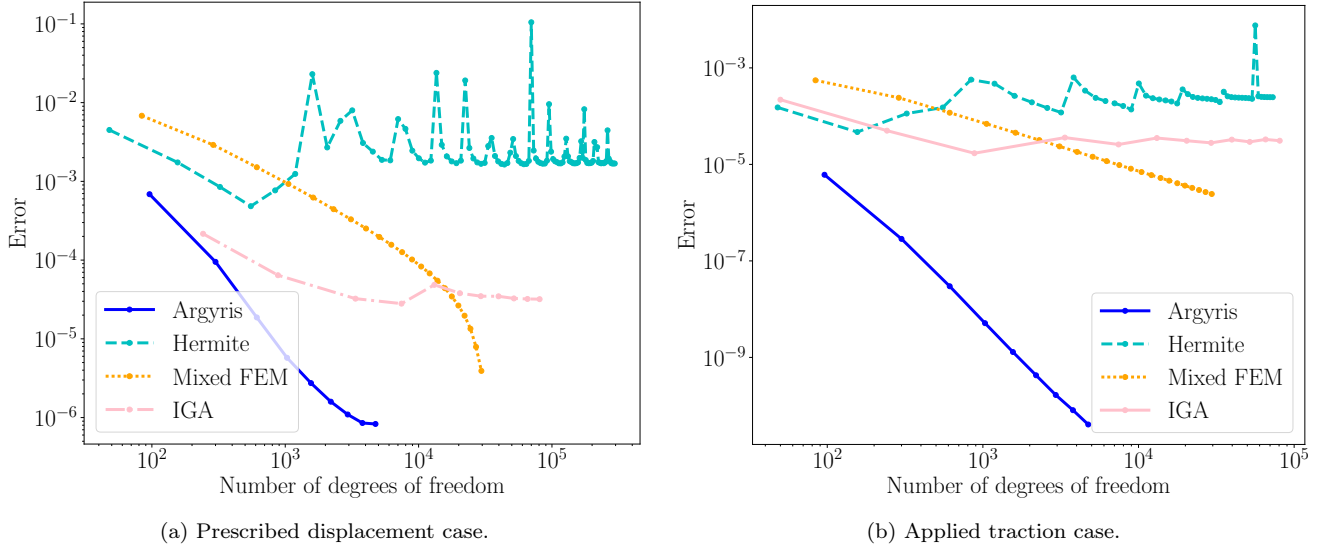


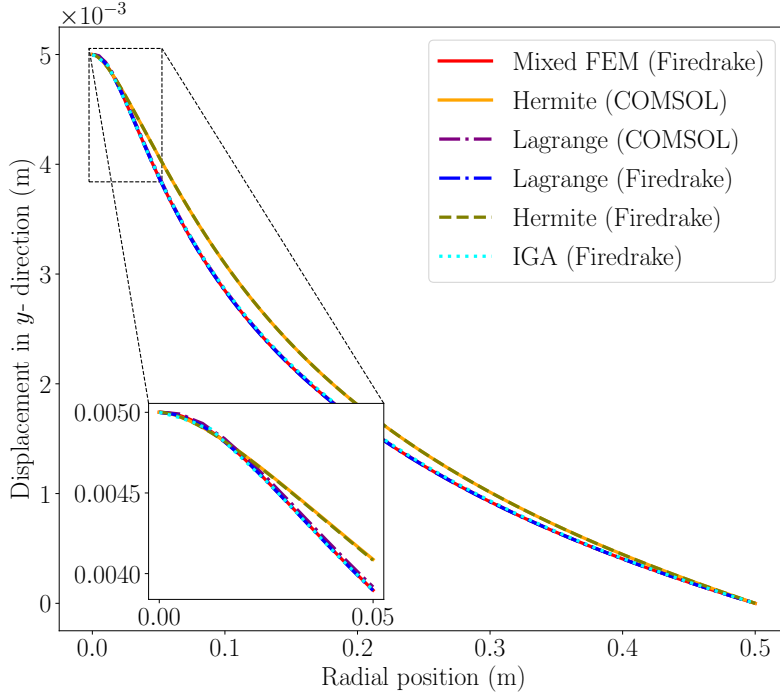
Figure 4: Error analysis on a log-log scale for finite elements in the simple shear deformation problem with prescribed displacement and applied traction

An analogous study has been conducted with the 1-D strain-gradient model of pull-out problem. By using different finite element formulations, we model rebar as embedded into a cylindrical concrete block of Young’s modulus  $E = 20$  GPa and Poisson’s ratio  $\nu = 0.2$ . In Table 2, all constitutive parameters are calculated by Eq. (26). The solution of this geometric nonlinear reduced order problem investigates the accuracy by using a linearization scheme. Herein, we use SNES scheme from PETSc libraries [60].

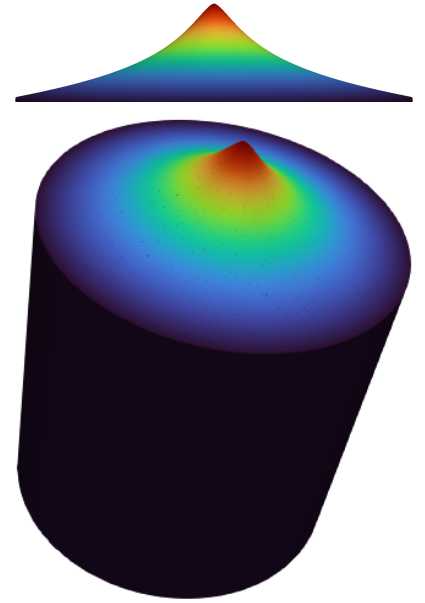
Table 2: Constitutive parameters for the pull-out problem.

| $c_1$ (MPa) | $c_2$ (MPa) | $c_3$ (N) | $c_4$ (N) | $c_5$ (N) | $c_6$ (N) | $c_7$ (N) |
|-------------|-------------|-----------|-----------|-----------|-----------|-----------|
| 5555.55     | 8333.33     | 6.20      | 1.55      | 8.37      | 2.02      | 8.37      |

The numerical simulations are performed using quadratic Lagrange, cubic Hermite elements, the mixed FE, and IGA with a 2nd-degree NURBS spline. In addition to the simulations on FEniCS and Firedrake, the problem is also investigated by COMSOL Multiphysics<sup>®</sup> using cubic Hermite and quadratic Lagrange elements. The weak form of the PDE is implemented by introducing the energy density in COMSOL Multiphysics<sup>®</sup>. In Fig. 5, the performed simulations are compared, providing the predicted displacements in the radial direction of the cylindrical block. For each element type, the problem is simulated with 5000 elements on FEniCS and Firedrake. It is clear that numerical simulations with Lagrange element, the mixed FE, and IGA compare each other very well. However, the displacement predicted by Hermite elements is notably different than other FE formulations. The same trend is observed for the simulations performed on COMSOL Multiphysics<sup>®</sup>. Overall, the predicted results on FEniCS and Firedrake compare well with those obtained by COMSOL Multiphysics<sup>®</sup>.



(a)



(b)

Figure 5: a) Comparison of the converged results of the strain-gradient elasticity solution of the pull-out problem  
b) 3-D illustration of deformation in the pull-out problem, captured in ParaView (scaled 50 times)

In order to investigate the convergence characteristics, a series of simulations is designed by using four levels of discretization. In this regard, the computational domain is divided into 5, 50, 500, and 5000 elements, respectively, to perform a convergence study. In Fig. 6, the convergence of each formulation is presented on a log-log scale using the  $L_1$  error norm as defined in (27). The most discretized solution, with 5000 elements, is considered the reference solution,  $u^{\text{ref}}$ . It is clear that monotonic convergence is observed for each element type for the 1-D non-linear strain-gradient model.

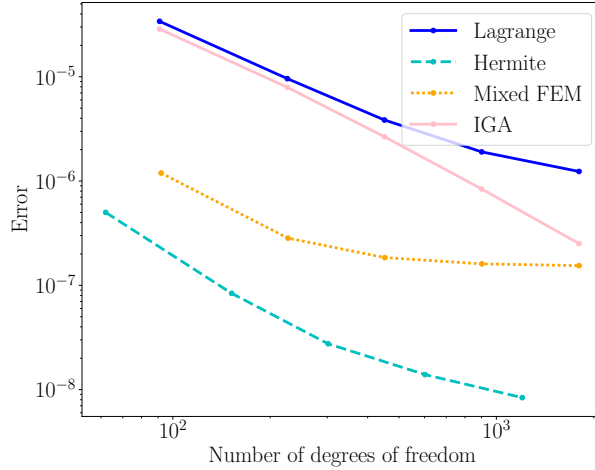


Figure 6: Convergence on a log-log scale for the pull-out problem

Furthermore, run-time performance of each finite element formulation is analyzed to assess their computational efficiency. Table 3 presents a comparison in terms of run-time, considering all the simulations examined in this study. For the 2-D model, it is clear that the mixed FE has the highest run-time for both cases, while IGA has the lowest. For the 1-D model, Lagrange elements have the highest run-time, followed by the mixed FE, Hermite elements, and IGA respectively. In this analysis, the number of degrees of freedom is kept constant for each case to ensure a fair comparison. Also, Hermite elements are excluded in the 2-D model due to their convergence behavior.

Table 3: Run-time performance of different finite element formulations

|  | Element Type | Number of Nodes | DOF | Runtime (sec) |
|--|--------------|-----------------|-----|---------------|
| <b>Case D:<br/>Prescribed Displacement</b> | Argyris      | 36              | 612 | 0.541         |
|  | Mixed FEM    | 36              | 612 | 0.768         |
|  | IGA          | 42              | 608 | 0.182         |
| <b>Case T:<br/>Applied Traction</b>        | Argyris      | 36              | 612 | 0.493         |
|  | Mixed FEM    | 36              | 612 | 0.751         |
|  | IGA          | 42              | 608 | 0.187         |
| <b>Case 3:<br/>Pull-out Problem</b>        | Lagrange     | 36              | 106 | 0.373         |
|  | Hermite      | 53              | 106 | 0.187         |
|  | Mixed FEM    | 36              | 107 | 0.337         |
|  | IGA          | 35              | 106 | 0.113         |

## 4 Conclusion

In this study, a numerical investigation is presented on the applicability of different finite element formulations within the framework of strain-gradient elasticity by using the open-source platforms FEniCS and Firedrake. To this end, two problems previously examined in the literature are investigated. A 2-D linear strain-gradient model is utilized for the simple shear of a plate. The simulations are performed for two different cases using Argyris, Hermite, a mixed FE, and IGA formulations. It is observed that Argyris and the mixed FE perform well, accurately predicting the problem under study, while Hermite and IGA lack the ideal convergence trends. Furthermore, a 1-D non-linear strain model is applied for the pull-out test, considering a rigid bar embedded into a cylindrical concrete block. For this problem, the 1-D simulations are performed using Lagrange, Hermite, the mixed FE, and IGA formulations. It is observed that all the finite element formulations exhibit monotonic convergence behavior for the 1-D model. Importantly, predicted displacement by Hermite elements is different than those obtained with other formulations. This discrepancy is also confirmed by simulations in COMSOL Multiphysics<sup>®</sup> for validation. Moreover, run-time performance of each formulation is analyzed to compare their computational efficiency.

## References

- [1] Bianca Maria Colosimo, Marco Grasso, Federica Garghetti, and Beatrice Rossi. Complex geometries in additive manufacturing: A new solution for lattice structure modeling and monitoring. *Journal of Quality Technology*, 54(4):392–414, 2022.
- [2] Gordon Zyla, Emilio Barchesi, Stefanos Mavrikos, Ivan Giorgio, Francesco dell’Isola, Costas Grigoropoulos, and Maria Farsari. 3d pantographic metamaterials at an extremely small length scale. In *Nanoscale and Quantum Materials: From Synthesis and Laser Processing to Applications 2024*, page PC128740G. SPIE, 2024.
- [3] Emilio Barchiesi, Stefanos Mavrikos, Ivan Giorgio, Costas Grigoropoulos, Maria Farsari, Francesco dell’Isola, and Gordon Zyla. Complex mechanical properties of 3d micro-metric pantographic metamaterials fabricated by two-photon polymerization. *Continuum Mechanics and Thermodynamics*, pages 1–12, 2024.
- [4] Minghao Bi, Lingwei Xia, Phuong Tran, Zhi Li, Qian Wan, Li Wang, Wei Shen, Guowei Ma, and Yi Min Xie. Continuous contour-zigzag hybrid toolpath for large format additive manufacturing. *Additive Manufacturing*, 55:102822, 2022.
- [5] Emilio Turco, Emilio Barchiesi, Andrea Causin, Francesco dell’Isola, and Margherita Solci. Harnessing unconventional buckling of tube origami metamaterials based on Kresling pattern. *International Journal of Solids and Structures*, page 112925, 2024.
- [6] Francisco Dos Reis and Nikolaos Karathanasopoulos. Deep learning, deconvolutional neural network inverse design of strut-based lattice metamaterials. *Computational Materials Science*, 244:113258, 2024.
- [7] Shivani Sriya Ambati and Ravindra Ambatipudi. Effect of infill density and infill pattern on the mechanical properties of 3d printed pla parts. *Materials Today: Proceedings*, 64:804–807, 2022.

- [8] Emilio Turco, Emilio Barchiesi, and Francesco dell’Isola. The long and winding road that leads to homogenisation of kresling origami. *International Journal of Non-Linear Mechanics*, 163:104756, 2024.
- [9] Davood Rahmatabadi, Elyas Soleyman, Mahshid Fallah Min Bashi, Mohammad Aberoumand, Kianoosh Soltanmohammadi, Ismaeil Ghasemi, Majid Baniassadi, Karen Abrinia, Mahdi Bodaghi, and Mostafa Baghani. 4d printing and annealing of petg composites reinforced with short carbon fibers. *Physica Scripta*, 99(5):055957, 2024.
- [10] Gokhan Aydin, M Erden Yildizdag, and Bilen Emek Abali. Strain-gradient modeling and computation of 3-d printed metamaterials for verifying constitutive parameters determined by asymptotic homogenization. In *Theoretical Analyses, Computations, and Experiments of Multiscale Materials: A Tribute to Francesco dell’Isola*, pages 343–357. Springer, 2022.
- [11] Reza Afshar, Simon Jeanne, and Bilen Emek Abali. Nonlinear material modeling for mechanical characterization of 3-d printed pla polymer with different infill densities. *Applied Composite Materials*, 30(3):987–1001, 2023.
- [12] Arnaldo Casalotti, Francesco D’Annibale, and Giuseppe Rosi. Optimization of an architected composite with tailored graded properties. *Zeitschrift für angewandte Mathematik und Physik*, 75(4):126, 2024.
- [13] Gokhan Aydin, B Cagri Sarar, M Erden Yildizdag, and B Emek Abali. Investigating infill density and pattern effects in additive manufacturing by characterizing metamaterials along the strain-gradient theory. *Mathematics and Mechanics of Solids*, 27(10):2002–2016, 2022.
- [14] Mihiro Torisaki, Masatoshi Shimoda, and Musaddiq Al Ali. Shape optimization method for strength design problem of microstructures in a multiscale structure. *International Journal for Numerical Methods in Engineering*, 124(8):1748–1772, 2023.
- [15] Rachele Allena, D Scerrato, AM Bersani, and I Giorgio. A model for the bio-mechanical stimulus in bone remodelling as a diffusive signalling agent for bones reconstructed with bio-resorbable grafts. *Mechanics Research Communications*, 129:104094, 2023.
- [16] Ivan Giorgio, Francesco dell’Isola, and David J Steigmann. Second-grade elasticity of three-dimensional pantographic lattices: theory and numerical experiments. *Continuum Mechanics and Thermodynamics*, pages 1–13, 2023.
- [17] Nurettin Yilmaz, M Erden Yildizdag, Francesco Fabbrocino, Luca Placidi, and Anil Misra. Emergence of critical state in granular materials using a variationally-based damage-elasto-plastic micromechanical continuum model. *International Journal for Numerical and Analytical Methods in Geomechanics*, 2024.
- [18] Maximilian Stilz, Francesco Dell’Isola, Ivan Giorgio, Victor A Eremeyev, Georg Ganzenmüller, and Stefan Hiermaier. Continuum models for pantographic blocks with second gradient energies which are incomplete. *Mechanics Research Communications*, 125:103988, 2022.
- [19] Jacek Chróścielewski, Francesco dell’Isola, Victor A Eremeyev, and Agnieszka Sabik. On rotational instability within the nonlinear six-parameter shell theory. *International Journal of Solids and Structures*, 196:179–189, 2020.

- [20] Jianqiu Tian, Yuanming Lai, Enlong Liu, and Chuan He. A thermodynamics-based micro-macro elastoplastic micropolar continuum model for granular materials. *Computers and Geotechnics*, 162:105653, 2023.
- [21] Anastasiya E Vilchevskaya, Elena N Vilchevskaya, Wolfgang H Müller, and Victor A Eremeyev. Modeling of blood flow in the framework of micropolar theory. *Continuum Mechanics and Thermodynamics*, 35(6):2337–2359, 2023.
- [22] Anil Misra, Luca Placidi, Francesco dell’Isola, and Emilio Barchiesi. Identification of a geometrically nonlinear micromorphic continuum via granular micromechanics. *Zeitschrift für angewandte Mathematik und Physik*, 72:1–21, 2021.
- [23] Pierre Seppecher and Lukáš Jakabčín. Asymptotic comparison of the strain-gradient and micromorphic models when loading forces are widely spread. In *Theoretical Analyses, Computations, and Experiments of Multiscale Materials: A Tribute to Francesco dell’Isola*, pages 253–272. Springer, 2022.
- [24] Mohammad Sarhil, Lisa Scheunemann, Peter Lewintan, Jörg Schröder, and Patrizio Neff. A computational approach to identify the material parameters of the relaxed micromorphic model. *Computer Methods in Applied Mechanics and Engineering*, 425:116944, 2024.
- [25] Ivan Giorgio, Michele De Angelo, Emilio Turco, and Anil Misra. A biot–cosserat two-dimensional elastic nonlinear model for a micromorphic medium. *Continuum Mechanics and Thermodynamics*, 32(5):1357–1369, 2020.
- [26] Ivan Giorgio, Francois Hild, Emaad Gerami, Francesco dell’Isola, and Anil Misra. Experimental verification of 2d cosserat chirality with stretch-micro-rotation coupling in orthotropic metamaterials with granular motif. *Mechanics Research Communications*, 126:104020, 2022.
- [27] Ivan Giorgio, Anil Misra, and Luca Placidi. Geometrically nonlinear cosserat elasticity with chiral effects based upon granular micromechanics. In *Sixty Shades of Generalized Continua: Dedicated to the 60th Birthday of Prof. Victor A. Eremeyev*, pages 273–292. Springer, 2023.
- [28] B Emek Abali, Wolfgang H Müller, and Victor A Eremeyev. Strain gradient elasticity with geometric nonlinearities and its computational evaluation. *Mechanics of Advanced Materials and Modern Processes*, 1:1–11, 2015.
- [29] Hua Yang, Dmitry Timofeev, B Emek Abali, Baotong Li, and Wolfgang H Müller. Verification of strain gradient elasticity computation by analytical solutions. *ZAMM-Journal of Applied Mathematics and Mechanics/Zeitschrift für Angewandte Mathematik und Mechanik*, 101(12):e202100023, 2021.
- [30] Victor A Eremeyev, Antonio Cazzani, and Francesco dell’Isola. On nonlinear dilatational strain gradient elasticity. *Continuum Mechanics and Thermodynamics*, 33:1429–1463, 2021.
- [31] Ivan Giorgio. Lattice shells composed of two families of curved kirchhoff rods: an archetypal example, topology optimization of a cycloidal metamaterial. *Continuum Mechanics and Thermodynamics*, 33(4):1063–1082, 2021.
- [32] Tomasz Lekszycki. Variational methods in structural optimization. *Encyclopedia of Continuum Mechanics*, pages 2643–2653, 2020.

- [33] Luca Placidi, Emilio Barchiesi, Anil Misra, and Ugo Andreaus. Variational methods in continuum damage and fracture mechanics. *Encyclopedia of continuum mechanics*, pages 2634–2643, 2020.
- [34] Anil Misra, Luca Placidi, and Emilio Turco. Variational methods for continuum models of granular materials. In *Encyclopedia of continuum mechanics*, pages 2611–2621. Springer, 2020.
- [35] Valerii Maksimov, Emilio Barchiesi, Anil Misra, Luca Placidi, and Dmitry Timofeev. Two-dimensional analysis of size effects in strain-gradient granular solids with damage-induced anisotropy evolution. *Journal of Engineering Mechanics*, 147(11):04021098, 2021.
- [36] Alessandro Ciallella, Francesco D’Annibale, Dionisio Del Vescovo, and Ivan Giorgio. Deformation patterns in a second-gradient lattice annular plate composed of “spira mirabilis” fibers. *Continuum Mechanics and Thermodynamics*, 35(4):1561–1580, 2023.
- [37] Salvatore Sessa, Emilio Barchiesi, and Luca Placidi. An implicit computational approach in strain-gradient brittle fracture analysis. *Mechanics Research Communications*, 136:104259, 2024.
- [38] Jean-Jacques Alibert, Pierre Seppecher, and Francesco Dell’Isola. Truss modular beams with deformation energy depending on higher displacement gradients. *Mathematics and Mechanics of Solids*, 8(1):51–73, 2003.
- [39] Francesco dell’Isola, Simon R Eugster, Roberto Fedele, and Pierre Seppecher. Second-gradient continua: From lagrangian to eulerian and back. *Mathematics and Mechanics of Solids*, 27(12):2715–2750, 2022.
- [40] F dell’Isola, E Turco, and E Barchiesi. 5 lagrangian discrete models: Applications to metamaterials. *Discrete and Continuum Models for Complex Metamaterials*, page 197, 2020.
- [41] U. Mühlich, B. E. Abali, and F. dell’Isola. Commented translation of Erwin Schrödinger’s paper ‘On the dynamics of elastically coupled point systems’(Zur Dynamik elastisch gekoppelter Punktsysteme). *Mathematics and Mechanics of Solids*, 26(1):1081286520942955, 2020.
- [42] K. K. Mandadapu, B. E. Abali, and P. Papadopoulos. On the polar nature and invariance properties of a thermomechanical theory for continuum-on-continuum homogenization. *Mathematics and Mechanics of Solids*, 26(11):1581–1598, 2021.
- [43] Navid Shekarchizadeh, Bilen Emek Abali, and Alberto Maria Bersani. A benchmark strain gradient elasticity solution in two-dimensions for verifying computational approaches by means of the finite element method. *Mathematics and Mechanics of Solids*, 27(10):2218–2238, 2022.
- [44] Nasrin Rezaei, M Erden Yildizdag, Emilio Turco, Anil Misra, and Luca Placidi. Strain-gradient finite elasticity solutions to rigid bar pull-out test. *Continuum Mechanics and Thermodynamics*, pages 1–11, 2024.
- [45] Leopoldo Greco, Domenico Castello, and Massimo Cuomo. An objective and accurate g1-conforming mixed bézier fe-formulation for kirchhoff–love rods. *Mathematics and Mechanics of Solids*, 29(4):645–685, 2024.



- [46] Florian Rathgeber, David A Ham, Lawrence Mitchell, Michael Lange, Fabio Luporini, Andrew TT McRae, Gheorghe-Teodor Bercea, Graham R Markall, and Paul HJ Kelly. Firedrake: automating the finite element method by composing abstractions. *ACM Transactions on Mathematical Software (TOMS)*, 43(3):1–27, 2016.
- [47] Thomas JR Hughes, John A Cottrell, and Yuri Bazilevs. Isogeometric analysis: Cad, finite elements, nurbs, exact geometry and mesh refinement. *Computer methods in applied mechanics and engineering*, 194(39-41):4135–4195, 2005.
- [48] Antonio Cazzani, Marcello Malagù, and Emilio Turco. Isogeometric analysis of plane-curved beams. *Mathematics and Mechanics of Solids*, 21(5):562–577, 2016.
- [49] J Schulte, M Dittmann, SR Eugster, S Hesch, T Reinicke, F dell’Isola, and C Hesch. Isogeometric analysis of fiber reinforced composites using kirchhoff–love shell elements. *Computer Methods in Applied Mechanics and Engineering*, 362:112845, 2020.
- [50] M Erden Yildizdag, I Tugrul Ardic, and Ahmet Ergin. An isogeometric fe-be method to investigate fluid–structure interaction effects for an elastic cylindrical shell vibrating near a free surface. *Ocean Engineering*, 251:111065, 2022.
- [51] David Kamensky and Yuri Bazilevs. tigar: Automating isogeometric analysis with fenics. *Computer Methods in Applied Mechanics and Engineering*, 344:477–498, 2019.
- [52] B. E. Abali, W. H. Müller, and F. dell’Isola. Theory and computation of higher gradient elasticity theories based on action principles. *Archive of Applied Mechanics*, 87(9):1495–1510, 2017.
- [53] B Emek Abali. Revealing the physical insight of a length-scale parameter in metamaterials by exploiting the variational formulation. *Continuum Mechanics and Thermodynamics*, 31(4):885–894, 2019.
- [54] B. E. Abali. Energy based methods applied in mechanics by using the extended noether’s formalism. *ZAMM - Journal of Applied Mathematics and Mechanics / Zeitschrift für Angewandte Mathematik und Mechanik*, 103:e202300020, 2023.
- [55] Emilio Barchiesi, Anil Misra, Luca Placidi, and Emilio Turco. Granular micromechanics-based identification of isotropic strain gradient parameters for elastic geometrically nonlinear deformations. *ZAMM-Journal of Applied Mathematics and Mechanics/Zeitschrift für Angewandte Mathematik und Mechanik*, 101(11):e202100059, 2021.
- [56] Manon Thbaut, Basile Audoly, and Claire Lestringant. Effective boundary conditions for second-order homogenization. *Journal of the Mechanics and Physics of Solids*, page 105707, 2024.
- [57] Lidiia Nazarenko, Rainer Glüge, and Holm Altenbach. Positive definiteness in coupled strain gradient elasticity. *Continuum Mechanics and Thermodynamics*, 33:713–725, 2021.
- [58] Francesco dell’Isola, Giulio Sciarra, and Stefano Vidoli. Generalized Hooke’s law for isotropic second gradient materials. *Proceedings of the Royal Society A: Mathematical, Physical and Engineering Sciences*, 465(2107):2177–2196, 2009.

- [59] Victor A Eremeyev, Sergey A Lurie, Yury O Solyaev, and Francesco dell’Isola. On the well posedness of static boundary value problem within the linear dilatational strain gradient elasticity. *Zeitschrift für angewandte Mathematik und Physik*, 71:1–16, 2020.
- [60] Satish Balay, Shrirang Abhyankar, Mark F. Adams, Steven Benson, Jed Brown, Peter Brune, Kris Buschelman, Emil M. Constantinescu, Lisandro Dalcin, Alp Dener, Victor Eijkhout, Jacob Faibussowitsch, William D. Gropp, Václav Hapla, Tobin Isaac, Pierre Jolivet, Dmitry Karpeev, Dinesh Kaushik, Matthew G. Knepley, Fande Kong, Scott Kruger, Dave A. May, Lois Curfman McInnes, Richard Tran Mills, Lawrence Mitchell, Todd Munson, Jose E. Roman, Karl Rupp, Patrick Sanan, Jason Sarich, Barry F. Smith, Stefano Zampini, Hong Zhang, Hong Zhang, and Junchao Zhang. PETSc Web page. <https://petsc.org/>, 2024.